Met. Mater. Int., Vol. 21, No. 5 (2015), pp. 799~804
doi: 10.1007/s12540-015-5215-y

Transformation Plasticity in Boron-Bearing Low Carbon Steel

Hye-Jin Jeong[1], Moon-Jo Kim[1], Dong-Wan Kim[1], Dong-Woo Suh[2], Jin-Keun Oh[3], and Heung Nam Han[1,*]

[1]Department of Materials Science and Engineering & Research Institute of Advanced Materials, Seoul National University, 1 Gwanak-ro, Gwanak-gu, Seoul 151-744, Korea
[2]Graduate Institute of Ferrous Technology, Pohang University of Science and Technology, 77 Cheongam-ro, Nam-gu, Pohang 790-784, Korea
[3]POSCO Technical Research Laboratories, 8 Pokposarang-gil, Gwangyang 545-875, Korea

(received date: 27 April 2015 / accepted date: 19 May 2015)

The transformation plasticity (TP), which indicates that permanent strain remains after solid-solid phase transformation, even under much smaller stress than the yield stress, has been described by a vacancy diffusion mechanism in the migrating interface during diffusional phase transformation. In this study, the influence of boron (B) addition on the TP of low carbon high strength steel was investigated through the observation of the B segregation in the phase interface between primary austenite phase and ferrite phase using secondary ion mass spectroscopy. The B segregation at the austenite-ferrite phase interface was confirmed to cause drastic decrease of the TP strain by comparison of the dilatation behavior of B-bearing and B-free steels under a tensile force during slow cooling, where the diffusional phase transformation occurs in B-bearing steel. Furthermore, it was also confirmed that the velocity of B diffusion is larger than the migration velocity of interface at the given temperature through a calculation based on Fick's law.

Keywords: segregation, plasticity, phase transformation, diffusion, SIMS

1. INTRODUCTION

The hot stamping technique has been highlighted as a breakthrough method to achieve both high strength and extensive formability, while also solving the springback problem of advanced high-strength steels (AHSSs) [1-6]. This method employs the high-temperature formation of an austenitic phase, followed by rapid cooling, which enables the austenitic phase to transform into a much harder martensitic phase. To produce a martensitic microstructure after hot stamping, steels with sufficient hardenability are required. Since the addition of a small amount of boron (B) remarkably increases the hardenability of low carbon, low alloy steels [7-10], B-bearing low carbon steels have been developed for hot stamping purposes.

The segregation of B atoms to austenite grain boundaries is known to reduce the grain boundary energy, thus causing retardation of the austenite-to-ferrite transformation [11,12]. In actual mill processes, however, the retardation of phase transformation induces incomplete phase transformation prior to coiling, resulting in asymmetric contraction during the cooling phase after coiling of the hot-rolled steel, which is a significant defect [13]. The asymmetric contraction of the hot coil is mainly caused by the transformation plasticity (TP), which indicates that permanent strain remains after the solid-solid phase transformation, even under much smaller stress than the yield stress [14,15]. Therefore, gaining an understanding of the TP behavior in B-bearing steel is very important to control the shape change of the hot coil.

Explanations of TP can be classified into three main groups according to their mechanisms: (1) weaker phase yielding [16], (2) favorable variant selection [15,17], and (3) accelerated diffusion on the migrating transformation interface [18]. The first of these explains macroscopically observed plasticity induced by volume mismatch between the hard phase and soft phase, which produces microscopic plasticity in the weaker phase [16]. The second important mechanism takes into account the anisotropy of the transformation strain during displacive transformation. Some of the authors suggested that the anisotropic transformation strain, based on the selectivity of some specific variants, increased due to the externally applied stress during the martensitic transformation [15,17,19]. Another microstructural theory for transformation strain is based on the diffusion mechanism of the migrating interface during diffusional phase transformation, which can be described as an accelerated Coble creep. Some researchers also derived a constitutive equation for TP as a thermally activated form by considering the atomic flux along the phase interface [18,20,21]. The asymmetric contraction in B-bearing low carbon steels might be closely related to the diffusion mechanism of the

*Corresponding author: hnhan@snu.ac.kr

migrating interface during the diffusional phase transformation. Though TP has been also called transformation induced plasticity (TRIP) in a lot of papers [15,18,19,22,23], TRIP has been frequently used as the concept of deformation induced martensitic transformation (DIMT) in literature [23,24]. In many cases, the austenitic steel with high strength-ductility balance based on DIMT is called TRIP steel [23-26]. Therefore, in this manuscript, the permanent strain during the solid-solid phase transformation is designated as TP for clear meaning.

In the present study, therefore, the influence of B addition to low carbon steel on the TP was investigated by observation of the B segregation in the phase interface using secondary ion mass spectroscopy (SIMS). The TP strain was measured by a tensile test under a constant load during sufficient slow cooling, where the diffusional phase transformation of B-bearing steel can occur. By comparison of the TP strains of B-bearing and B-free steels, the influence of B addition on the TP was quantitatively analyzed based on the constitutive equation for TP.

2. EXPERIMENTAL PROCEDURES

Two kinds of low-carbon steels (B-bearing and B-free steels) were used in the experiments, which contained almost the same chemical compositions except for B, as listed in Table 1. To determine the phase transformation kinetics of the steels during cooling, rectangular dilatometric specimens were prepared with the width of 3 mm, thickness of 3 mm and length of 10 mm. The dilatometric experiments were performed using a transformation dilatometer (Theta, Dilatronic III), which can control the specimen temperature with an induction heating/Ar blowing system. The dilatometric data were obtained with a linear variable displacement transducer (LVDT). The specimens were austenitised at 900 °C for 10 min under vacuum conditions, and then cooled down to room temperature at the rates of 0.015, 0.03, 0.1 and 0.3 °C/sec. These cooling rates were chosen as being sufficiently slow, whereat the asymmetric contraction of hot coil can occur due to TP [13].

To measure the TP strain for the same cooling rates, a uniaxial tensile tester (Instron 2416) equipped with a high temperature furnace was utilized under the constant stress condition of 30 MPa. To supply the uniaxial tensile load to cylindrical specimens with a diameter of 4 mm and gauge length of 25 mm, the weight of 38.5 kg was employed. The temperature of the furnace was precisely controllable to achieve the slow cooling rates. The TP strain was determined from the length change between the initial and final specimens after cooling.

The B distribution and segregation patterns were determined with the aid of nano-SIMS (Nano-SIMS 50, CAMECA), which is known to be an effective technique for providing a more quantitative understanding of the B distribution in steel [27]. Nano-SIMS measurements were carried out using a Cs+ beam with an impact energy of 16 keV [28]. An ion probe with 0.4 pA was sputtered over a square area of 60 by 60 μm, and the negatively charged secondary ions emitted from the surface were used to obtain mass-resolved ion images. When analyzing the B distribution, the $^{11}B^{16}O_2$ signal on mass 43, which is the strongest B channel, was recorded. To clarify the distribution of B and C, the SIMS images were compared with the optical microscope images obtained at the same regions.

3. RESULTS AND DISCUSSION

Figure 1 shows the experimental dilatometric curves of B-bearing and B-free steels measured during cooling from 900 °C at several slow cooling rates, where the asymmetric contraction of hot coil can occur due to TP [13]. It was confirmed that the transformation kinetics clearly slowed down with increasing cooling rate. In addition, the continuous cooling transformation behavior of B-bearing steel (closed symbol) indicates that the start of transformation was further depressed in comparison with the B-free steel (open symbol). The retardation effect of B on the austenite-to-ferrite transformation is known to be caused by the segregation of B along the aus-

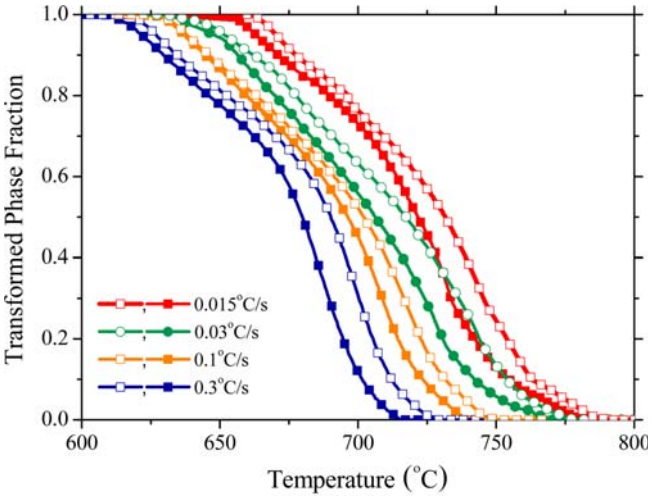

Fig. 1. Phase transformation kinetics of B-free and B-bearing steels under various cooling rates. Open and closed symbols indicate B-free and B-bearing steels, respectively.

Table 1. Chemical composition of the investigated steels (wt%)

Steels	Alloying elements					
	C	Si	Mn	Ti	N	B
B-free	0.227	0.26	1.21	0.04	0.0030	-
B-bearing	0.222	0.26	1.21	0.04	0.0047	0.0025

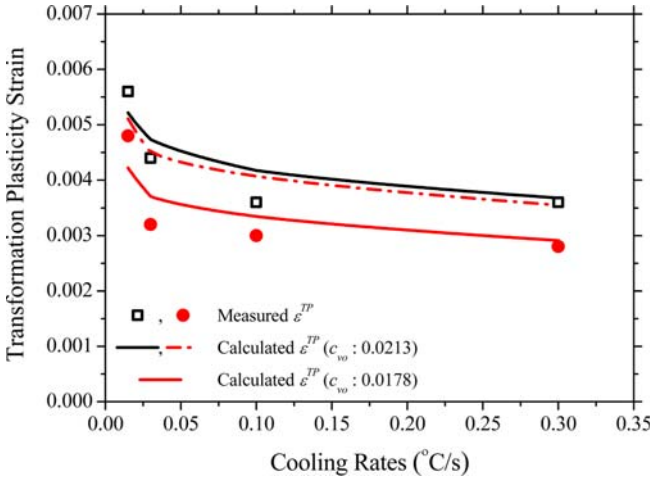

Fig. 2. Measured transformation plasticity (TP) strain ε^{TP} (symbols) under various cooling rates and calculated ε^{TP} (lines) values based on Eq. (1). Open and closed symbols indicate B-free and B-bearing steels, respectively.

tenite grain boundaries [11,12]. It should be noted that the overall transformation temperature in B-bearing steel was clearly lower than that in B-free steel at the cooling rates tested. The experimental kinetics data in Fig. 1 were used for the later calculation of the TP strain.

In order to investigate the effect of B on the TP, the TP strains were measured at the same cooling rates under the constant stress condition of 30 MPa. The TP strains for B-free and B-bearing steels were presented in Fig. 2 as open and close symbols, respectively. The TP strain of B-free steel was found to be much higher than that of the B-bearing steel under the given cooling rates. In both steels, TP strain was increased with decreasing cooling rate. The cooling rate effect on TP strain can be understood by examining the difference of the transformation temperature, which may be described by the thermally activated TP model considering atomic flux along the phase interface [18]. The diffusion-controlled TP strain rate $\dot{\varepsilon}^{TP}$ under externally applied stress was derived as follows:

$$\dot{\varepsilon}^{TP} = \frac{1}{3}\frac{d_0}{\delta}\dot{X}\frac{\sigma\Omega}{k_B T}c_{v0}\exp\left(-\frac{Q_f}{k_B T}\right) \quad (1)$$

where d_0, δ, and Ω represent the initial grain size of the parent phase, the effective thickness of the interface and the volume of the vacancy, respectively. The Boltzmann constant, k_B, has a value of 1.38×10^{-23} J/K. c_{v0} is a dimensionless constant determined by the change in thermal entropy associated with the formation of vacancies, while Q_f is the formation enthalpy of the vacancy at the phase interface. σ and $\dot{X}$ indicate the applied stress and transformation rate, respectively. The initial grain size of the austenite phase was found to be 30 μm for both steels. The parameters in Eq. (1) of the vacancy volume (Ω) and the effective thickness of the interface (δ) were 1.21×10^{-29} m^3 [29] and 1 nm, respectively. The formation enthalpy of the vacancy at the austenite and ferrite interface (Q_f) in conventional low carbon steels was reported to be 80 kJ/mol [18].

The value of c_{v0} for the B-free steel was adjusted using the constrained Rosenbrock technique [30] as an optimization procedure, which was performed while systematically changing the constants until the sum of the squared differences between the experimental and calculated data reached a minimum. The black solid line in Fig. 2 indicates the TP strains of B-free steel at the various cooling rates calculated by the time integration of Eq. (1). The calculated results revealed decrease of the transformation temperature with increasing cooling rate, thus leading to a gradual decrease of the TP strain. This phenomenon reflects the thermally activated characteristics of TP, and Eq. (1) successfully described the thermally activated behavior of TP strain. However, the TP strains (red dotted line) for B-bearing steel, which were calculated based on the same c_{v0} value as B-free steel, were much higher than the experimental data. Though the transformation temperature of B-bearing steel is lower than that of B-free steel, as shown in Fig. 1, and smaller TP strain can be expected due to B-bearing, a considerable difference between the calculated and measured data was observed. Because c_{v0} in Eq. (1) indicates the change in thermal entropy associated with the formation of vacancies, it can be determined that there was a smaller value of c_{v0} in B-bearing steel due to the reduction of the grain boundary energy or phase interface energy caused by the segregation of B atoms to the austenite grain boundary or phase interface during the slow cooling. The red solid line in Fig. 2 indicates the TP strains for B-bearing steel optimized by the time integration of Eq. (1). The c_{v0} value for B-bearing steel was determined to be much smaller compared with the B-free steel, while the calculated TP strains also successfully described the thermally activated behavior.

To verify the smaller value of c_{v0} in the B-bearing steel, the B segregation at the phase interface, as well as the austenite grain boundary, should be observed during cooling. In this study, the B distribution during cooling was investigated with the aid of nano-SIMS. Figures 3(a) to (c) show the optical micrograph, the secondary $^{12}C^-$ ion map, and the secondary $^{11}B^+$ ion map, respectively, for the B-bearing steel quenched from 900 °C. Within an individual SIMS image, the level of brightness is proportional to the number of counts per one pixel in the image, thus the relative comparison of $^{11}B^+$ and $^{12}C^-$ ion in steel could be conducted. The microstructure was determined to be in the martensite phase, and the carbon was well distributed throughout the whole specimen. From Fig. 3(c), it could be confirmed that the B was mostly segregated at the primary austenite grain boundary. Therefore, it could easily be understood that the segregation of B retards the austenite-to-ferrite phase transformation, as shown in Fig. 1.

Figures 3(d) to (f) show the optical micrograph, the secondary $^{12}C^-$ ion map, and the secondary $^{11}B^+$ ion map, respec-

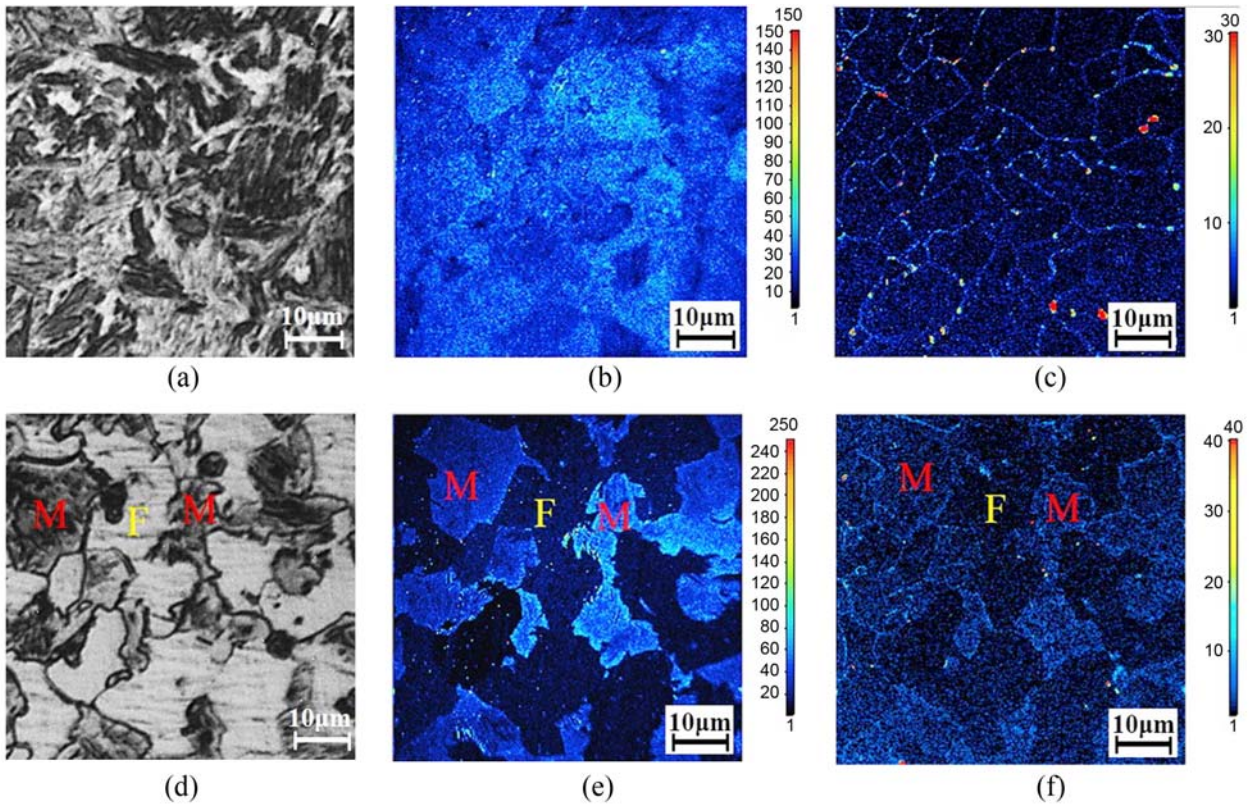

Fig. 3. Optical micrographs, carbon ion ($^{12}C^-$) micrographs and boron ion ($^{11}B^+$) micrographs of B-bearing steel obtained in the same region for the cooling rates of (a, b, and c) 40 °C/s and (d, e and f) 0.3 °C/s, respectively. F and M in (d), (e), and (f) indicate ferrite and martensite, respectively. The source used for analysis of the carbon and boron distribution was Cs^+ at the impact energy of 16 keV.

tively, for the B-bearing steel, which was cooled at 0.3 °C/sec from 900 °C to 680 °C and then quenched to room temperature. The ferrite fraction was almost 50%, which is accordance with the dilatometric analysis in Fig. 1. Because the martensite phase in Fig. 3(d) was the remaining austenite phase at 680 °C, the carbon content in the martensite was much higher than that in the transformed ferrite, as shown in Fig. 3(e). From the optical micrograph and the carbon distribution shown in Figs. 3(c) and (d), the phase interface between primary austenite and ferrite could be identified. After identification of the phase interface, the B segregation at the phase interface, as well as the austenite grain boundary, could be confirmed, as shown in Fig. 3(f).

To clarify the possibility of segregation of B at the phase interface, the velocity of B diffusion was calculated at various temperatures of 600, 700 and 800 °C, which cover over a range of phase transformation temperatures, and compared with the migration velocity of the phase interface during phase transformation. The concentration change of B solute from the grain boundary of primary austenite over time was described under the isothermal condition by Fick's law as follows [31]:

$$C = \frac{M}{2\sqrt{(\pi Dt)}}\exp\left(-\frac{x^2}{4Dt}\right) \quad (2)$$

where t, D, and M are the time for diffusion, the diffusion coefficient of B in austenite, and the amount of solute which made the total concentration of 1, respectively. x indicates the diffusion distance from the grain boundary. The formula for D can be expressed as follows [32]:

$$D = 2.3\times10^{-7}\exp\left(-\frac{79560}{RT}\right) \quad (3)$$

where R is the universal gas constant, 8.3144 $JK^{-1}mol^{-1}$, and T is the absolute temperature. By tracking the position of 70% of the B concentration for a given temperature and differentiating the position with respect to time, the velocity of B diffusion could be obtained, as shown in Fig. 4.

As for the migration velocity of the phase interface during phase transformation, the spherical geometry was used as a single austenite grain undergoing the diffusional phase transformation. It was assumed that the transformation started at the austenite grain boundary, which had the initial grain size of d_0, and that the new ferrite phase grew to the center of the austenite phase. The relationship between the grain diameter and the transformed ferrite fraction, X, can then be expressed as [18]:

$$\frac{d_p^3}{d_0^3} = (1-X) \quad (4)$$

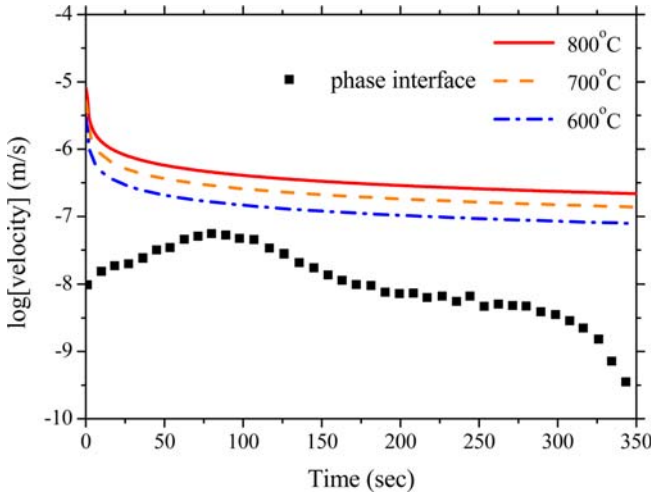

Fig. 4. Comparison between the calculated migration velocities (symbols) of the phase interface during phase transformation and the calculated boron diffusion velocities (lines) at various temperatures.

where d_p is the diameter of the parent austenite phase during the transformation. The migration velocity of the interface, v, can be expressed as [18]:

$$v = -\dot{d}_p = \frac{1}{3} d_0 (1-X)^{-2/3} \dot{X} \tag{5}$$

where the dot indicates the time derivative. Finally, the migration velocity of the interface could be obtained, as shown in Fig. 4. The velocity of B diffusion was found to be about 1-2 orders of magnitude larger than the migration velocity of the interface during phase transformation. This confirmed that the segregation of B at the phase interface can occur during phase transformation under the given cooling conditions.

A considerable amount of experimental and theoretical work has already been carried out on the segregation of B atoms at the grain boundary or moving grain boundary in metals and alloys. In particular, it was previously reported that strong interactions exist between the B atoms and vacancies [33-35]. Because a number of vacancies exist in the grain boundary or the phase interface and B has a tendency to remain there for appreciable periods of time [36], the probability of B segregation occurring at the interface will obviously increase, as shown in Figs. 3 and 4. Therefore, B segregation occupying the vacancies at the interface could lead to reduction of the thermal entropy associated with vacancies. This causes the value of c_{v0} in Eq. (1) to decrease. As a result, the TP of B-bearing steel is decreased compared with B-free steel, which seemed to match well with the experimental results shown in Fig. 2.

4. CONCLUSIONS

In the present study, the transformation plasticity (TP) of B-bearing and B-free steels was investigated. From the dilatometric analysis, it was confirmed that the phase transformation of B-bearing steel was retarded comparing with B-free steel, which was in good agreement with many previously reported observations. From analysis of the B distribution through nano-SIMS, the segregation of B at the phase interface between the primary austenite and ferrite phase was detected. Furthermore, calculation of the velocity of B diffusion and the migration velocity of interface confirmed that the segregation of B at the phase interface could sufficiently occur under the given cooling conditions.

Finally, the TP strains, which were measured by a tensile test under a constant load, could be described well by the thermally activated TP model with consideration of atomic flux along the phase interface. The measured transformation plasticity (TP) strain of B-bearing steel was considerably lowered than that of B-free steel. This can be understood by considering the segregation of B at the phase interface, which caused decrease of the thermal entropy associated with the formation of vacancies at the interface.

ACKNOWLEDGEMENT

This work was supported by the Basic Science Research Program through the National Research Foundation of Korea (NRF) funded by the Ministry of Science, ICT and Future Planning (NRF-2013R1A2A2A01008806).

REFERENCES

1. M. G. Lee, D. Y. Kim, C. M. Kim, M. L. Wenner, and K. S. Chung, *Int. J. Plast.* **21**, 915 (2005).
2. M. Merklein and J. Lechler, *J. Mater. Process. Technol.* **177**, 452 (2006).
3. P. F. Bariani, S. Bruschi, A. Ghiotti, and A. Turetta, *CIRP Ann.* **57**, 265 (2008).
4. H. H. Cho, Y. G. Cho, D. W. Kim, S. J. Kim, W. B. Lee, and H. N. Han, *ISIJ Int.* **54**, 1646 (2014).
5. C. W. Ji, I. D. Choi, Y. D. Kim, and Y. D. Park, *Korean J. Met. Mater.* **52**, 931 (2014).
6. J. D. Shim, *Korean J. Met. Mater.* **26**, 248 (2013).
7. B. M. Kapadia, R. M. Brown, and W. J. Murphy, *Trans. Met. Soc. AIME* **242**, 1689 (1968).
8. J. E. Morral, and T. B. Cameron, *Metall. Trans. A* **8**, 1817 (1977).
9. M. J. Kim, H. H. Cho, S. H. Kim, S. M. Nam, S. H. Lee, M. B. Moon, and H. N. Han, *Met. Mater. Int.* **19**, 629 (2013).
10. H. S. Yim, W. Y. Jung, and B. C. Hwang, *Korean J. Met. Mater.* **26**, 241 (2013).
11. K. Yamamoto, T. Hasegawa, and J. I. Takamura, *ISIJ Int.* **36**, 80 (1996).
12. V. V. Levitin, *Phys. Metals Metallography* **10**, 294 (1960).
13. H. H. Cho, Y. G. Cho, Y. R. Im, J. K. Lee, J. H. Kwak, and H. N. Han, *J. Mater. Process. Technol.* **210**, 907 (2010).

14. H. N. Han and J. K. Lee, *ISIJ Int.* **42**, 200 (2002).
15. H. N. Han and D. W. Suh, *Acta Mater.* **51**, 4907 (2003).
16. G. W. Greenwood and R. H. Johnson, *Proc. R. Soc. London A* **286**, 403 (1965).
17. C. L. Magee, *Ph. D. Thesis*, Carnegie Institute of Technology, Pittsburgh PA (1966).
18. H, N. Han, J. K. Lee, D. W. Suh, and S. J. Kim, *Philos. Mag*. **87**, 159 (2007).
19. H. N. Han, C. G. Lee, C. S. Oh, T. H. Lee, and S. J. Kim, *Acta Mater*. **52**, 5203 (2004).
20. H. N. Han, J. K. Lee, and S. J. Kim, *Mater. Lett*. **59**, 158 (2005).
21. H. N. Han, S. J. Kim, M. Y. Kim, G. S. Kim, D. W. Suh, and S. J. Kim, *Philos. Mag.* **88**, 1811 (2008).
22. F. D. Fischer, G. Reisner, E. Werner, K. Tanaka, G. Cailletaud, and T. Antreter, *Int. J. Plast.* **16**, 723 (2000).
23. H. N. Han, C. S. Oh, G. S. Kim, and O. J. Kwon, *Mater. Sci. Eng. A* **499**, 462 (2009).
24. J. Y. Choi, S. W. Hwang, M. C. Ha, and K. T. Park, *Met. Mater. Int*. **20**, 893 (2014).
25. T. H. Lee, H. Y. Ha, J. Y. Kang, J. O. Moon, C. H. Lee, and S. J. Park, *Acta Mater.* **61**, 7399 (2013).
26. S. Zaefferer, J. Ohlert, and W. Bleck, *Acta Mater.* **52**, 2765 (2004).
27. J. N. Kim, S. U. Lee, H. D. Kwun, K. S. Shin, and C. Y. Kang, *Met. Mater. Int.* **20**, 1067 (2014).
28. J. B. Seol, B.-H. Lee, P. Choi, S.-G. Lee, and C. G. Park, *Ultramicroscopy* **132**, 248 (2013).
29. H. J. Frost and M. F. Ashby, *Deformation Mechanism Maps*, p. 182, Pergamon Press, London (1982).
30. J. L. Kuester and J. H. Mize, *Optimization Techniques with Fortran*, p.386, McGraw-Hill, New York (1973).
31. D. A. Porter and K. E. Easterling, *Phase Transformations in Metals and Alloys 2nd ed.*, pp. 75-79, Chapman & Hall, London (1992).
32. F. H. Wohlbier, *Diffusion and Defect Data (Engl. Transl.) Vol.3*, p.133, Diffusion Information Center, Ohio (1969).
33. T. M. Williams, A. S. Stoneham, and D. R. Harries, *Metal. Sci*. **10**, 14 (1976).
34. L. Karlsson, H. Norden, and H. Odelius, *Acta Mater.* **36**, 1 (1988).
35. D. J. Mun, E. J. Shin, K. C. Cho, J. S. Lee, and Y. M. Koo, *Metall. Trans. A* **43A**, 1639 (2012).
36. M. Jahazi and J. J. Jonas, *Mater. Sci. Eng. A* **355**, 49 (2002).